Journal of Naval Architecture and Marine Engineering
December, 2024
http://dx.doi.org/10.3329/jname.v21i2.37895 *http://www.banglajol.info*

USING CFD TO INVESTIGATE THE EFFECT OF DUCTS ON PROPELLER PERFORMANCE

Ngo Van He[1], Nguyen Chi Cong[2] and Luong Ngoc Loi[1]
[1]School of Mechanical Engineering, Hanoi University of Science and Technology, No.1, Dai Co Viet, 10000, Hanoi, Vietnam, he.ngovan@hust.edu.vn, loi.luongngoc@hust.edu.vn.
[2]Mechanical Engineering Institute, Vietnam Maritime University, 180000, Haiphong, Vietnam, congnc.vck@vimaru.edu.vn

Abstract:

Ducted propellers find widespread application across various vessels, such as fishing vessels, trawlers, and submarines, owing to their proven efficiency in propulsion systems. This paper explores the hydrodynamic impact of ducts on propeller performance through the application of a commercial Computational Fluid Dynamics (CFD) code. Additionally, an analysis of various turbulence models, including RNG k-ε, SST k-ω, and transition SST k-ω, was conducted to understand their effects on the calculated results. The propeller under consideration in this study possesses significant parameters: a diameter of 3.65 m, operating at 200 rpm, with an average pitch angle of 2.459 m and a boss ratio of 0.1730. The duct employed in the ducted propeller system features a NACA 4415 profile, chosen for its favorable hydrodynamic characteristics, making it well-suited for the propeller duct. The methodology involved the construction, meshing, and refinement of the geometry model for both the open water propeller and the ducted propeller system. Subsequently, the performance of these systems was analyzed using the RNG k-ε, SST k-ω, and transition SST k-ω RANS turbulence models. The study delves into the effects of the duct on the propeller's hydrodynamic features, as well as the influence of different turbulence models on the obtained results. The computed results presented encompass pressure distribution, hydrodynamic characteristics, and velocity profiles behind the propeller in various scenarios. The paper concludes with a comprehensive discussion of the effects of the duct on hydrodynamic features and the impact of different turbulence models on the results, providing valuable insights into the interplay between ducts and propeller performance.

Keywords: Ducted propeller, propulsion, hydrodynamics, CFD, turbulence model.

1. Introduction

Ducted propellers, comprising an annular duct and a propeller assembly, have found application in various vessels, including tugs, push-boats, trawlers, and torpedoes. Their utilization extends to larger vessels such as tankers and bulk carriers, where they enhance hydrodynamic characteristics, especially in adverse conditions. Two predominant types of ducts exist in practice, accelerating and decelerating (Bhattacharyya *et al*, 2015, Bontempo *et al*, 2016, Dai *et al*, 2021, Kao and Liao, 2022, Majdfar *et al*, 2017, Razaghian and Ghassemi, 2016, Villa *et al*, 2020, Zondervan *et al*, 2006. In an accelerating duct, the flow velocity expands due to hydrodynamic performances of the duct, resulting in a lower drag force compared to the lift force, particularly in challenging conditions. Combining an accelerating duct with the propeller can mitigate propeller damage and enhance propulsive efficiency by axial losses during bollard conditions. Conversely, decelerating ducts diminish propulsive efficiency but mitigate cavitation initiation and reduce the risk of vibration. The decelerating duct is occasionally employed as a pump-jet system in specialized marine vehicles, such as torpedoes (Suryanarayana *et al*, 2010) . In the examination of propeller performance, Reynolds-Averaged Navier-Stokes (*RANS*) methods have gained prominence for calculating ducted propeller systems, demonstrating success in predicting open water characteristics, notably for well-known KA-Series (Abdel-Maksoud and Heinke, 2002, Caja *et al*, 2001, Krasilnikov *et al*, 2007). In 2013, Takinaci and Taralp (2021) utilized Computational Fluid Dynamics (*CFD*) to predict propeller noise during operation.

Numerous numerical methods have been proposed to study ducted propellers based on potential flow theory. For instance, Kerwin *et al.*, (1987) combined a panel method, also known as Boundary Element Method (BEM), with a vortex lattice method to model the duct for the propeller. Lee and Kinnas (2006) introduced another panel method specifically for the complete ducted propeller system operating in unsteady flow conditions, encompassing blade sheet cavitation. Both approaches incorporated a transpiration velocity model for the gap flow between propeller blade tip and duct inner surface and analyzed the duct with a sharp trailing edge. While

1813-8235 (Print), 2070-8998 (Online) Received on: August 2018

the use of a non-viscous flow model for ducted propellers was found beneficial, limitations were noted in regions where viscosity effects cannot be ignored, particularly in the gap flow. This region significantly influence propeller and duct circulation distribution, as well as the distribution of loading between propeller and duct (Baltazar and Falcao, 2009, Baltazar *et al*, 2012). Moreover, substantial interaction between the vortices shed from the propeller blade tips and the boundary layer developing on the duct inner side, previously overlooked in potential flow methods, was highlighted by Rijpkema and Vaz (2011) .

Koh *et al* (2015) conducted research to design a duct section profile for enhanced characteristics of fishing vessels propellers at a highly advanced coefficient, surpassing efficient of the 19A ducted propeller. Their experimental results demonstrated a maximum 23% increase in propeller thrust at highly advanced ratios compared to the 19A ducted propeller. Neural networks were employed to analyze propeller open water characteristics, specifically the four-blade KA-Series located in the 19A duct. A two-layered, feed-forward neural network system was trained to design this solver system (Motallebi-Nejad *et al*, 2017, Razaghian and Ghassemi, 2016) . Ngo *et al* (2015) utilized the Multi Block Hybrid Mesh (*MBHM*) and Reynolds Stress Model (*RSM*) methods to study the hydrodynamic characteristic of the ducted propeller, comparing numerical results with the Standard k – ε two-equation model for the two JD7704+KA4-55 propellers. The conclusion was that MBHM and RSM methods are more suitable for determining ducted propeller hydrodynamic characteristics (Cong *et al*, 2018, Loi *et al*, 2019, Ngo *et al*, 2015) . Furthermore, Majdfar *et al* (2015) employed a RANS equation solver to investigate the influence of various shape of nozzle 19A, duct length and angle on the Kaplan propeller. Additionally, Ghassemi *et al* (2016) extended the calculations of the hydrodynamic characteristics of a ducted propeller operating in oblique flow.

In the current work, the RNG *k-ε*, SST *k-ω*, and Transition SST *k-ω* models were utilized to predict the hydrodynamic performance of both open and ducted propellers. The simulation results, encompassing pressure distribution, velocity field, and open water characteristics, were compared for the ducted propeller. This analysis sheds light on the effects of a duct and different turbulence models on the hydrodynamic characteristic of a propeller.

2. Theoretical foundation

2.1 Propeller's hydrodynamic features

According to the theory of wing, the propeller blade is conceptualized as being divided in to numerous elementary strips, as illustrated in Fig. 1. Examining a blade element, depicted in Fig. 1, each of these elementary strips can be treated as an airfoil subject to a resultant incident velocity *W*. The resultant incident velocity is considered to consist of an axial velocity *V* in combination with a rotational velocity Ωr, which linearly varies up the blade.

This section will consequently encounter lift and drag forces arising from the interplay of the incidence angle and the section's zero lift angle. It can be inferred that, given a specific section geometry, the elemental thrust and torques can be expressed as follows (Abbott, 1959, Breslin and Andersen, 1994):

$$dT = \frac{1}{2}\rho.Z.c.W^2(c_l.\cos\beta - c_d.\sin\beta)dr$$
$$dK = \frac{1}{2}\rho Zc.W^2(c_l.\sin\beta + c_d.\cos\beta)rdr \quad (1)$$

Therefore, the thrust and torque of a propeller can be found by integrating formula.

$$T = \int_{r_h}^{r_t}\frac{1}{2}\rho.Z.c.W^2(c_l.\cos\beta - c_d.\sin\beta)dr$$
$$Q = \int_{r_h}^{r_t}\frac{1}{2}\rho.Z.c.W^2(c_l.\sin\beta + c_d.\cos\beta)rdr \quad (2)$$

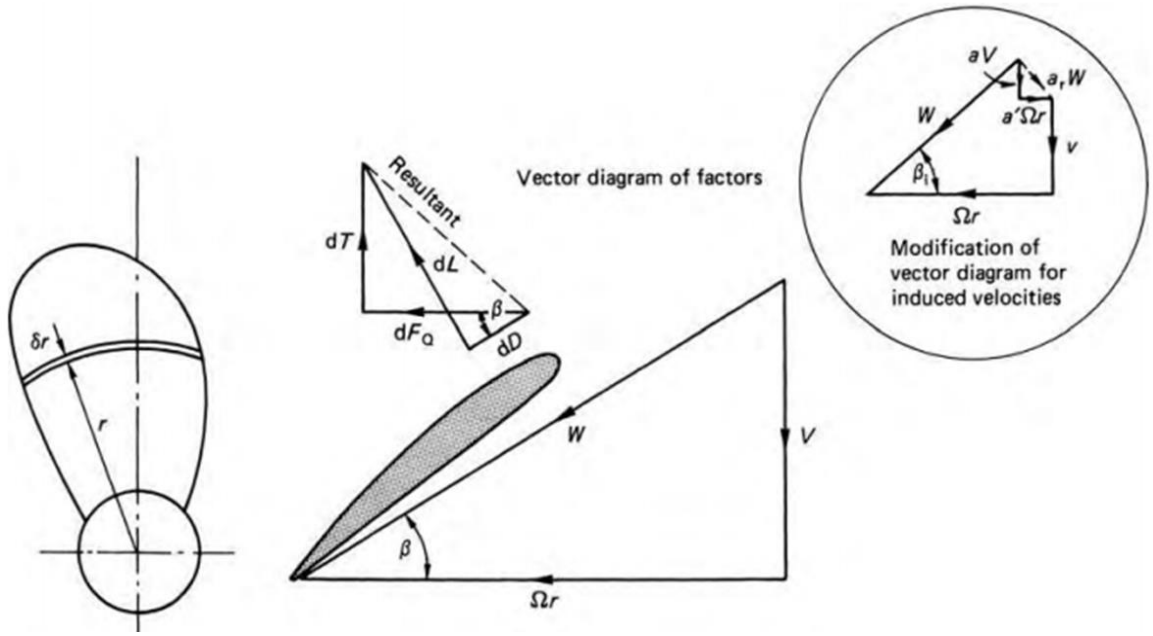

Fig. 1: Blade element of the propeller's blade Abbott (1959)

Where, Z and c represent the number of blades and the chord length of the section, respectively. c_l, c_d denote the lift and drag coefficients of the profile at the specific radius.

From the Equation (2), we determine the characteristic coefficients of a propeller, including thrust, torque, and efficiency coefficient. These hydrodynamic coefficients for the free propeller can be defined as follows:

$$K_T = \frac{T}{\rho n^2 D^4} \quad K_Q = \frac{Q}{\rho n^2 D^5} \quad J = \frac{V_a}{nD} \quad \eta_0 = \frac{K_T.J}{K_Q.2\pi} \tag{3}$$

In the case of a ducted propeller, the total thrust of the system comprises two components: the thrust generated by the propeller and the thrust produced by the duct. Consequently, the hydrodynamic characteristics differ slightly from those of a free propeller. These components can be defined as follows.

$$K_{Tp} = \frac{T_p}{\rho n^2 D^4}; K_{Td} = \frac{T_d}{\rho n^2 D^4}; K_Q = \frac{Q}{\rho n^2 D^5};$$
$$J = \frac{V_a}{nD}; \eta_0 = \frac{\left(K_{Tp} + K_{Td}\right).J}{K_Q.2\pi} \tag{4}$$

Where J is the advanced ratio, V_a is the axial velocity, n is the rotating speed, D is the diameter of the propeller, T_p and T_d are the thrusts of the propeller and duct, respectively, Q is the torque of the propeller, ρ is the density of fluid. K_{tp} and K_{td} are the thrust coefficients of the propeller and duct, respectively. K_Q is the torque coefficient of the propeller, η_o is the efficiency of the ducted propeller.

2.2 Fundamental equations

As we are aware, numerous fluid related problems are tackled solving the Navies-Stokes equations to determine the pressure and velocity distribution fields along with other crucial parameters. In this paper, the problem was addressed through the application of the finite volume method using the commercial CFD code ANSYS- Fluent. The fundamental equations employed include the continuity equation and the Reynolds-Averaged Navies-Stokes (*RANS*) equation in rotating coordinate system, expressed as follows (ANSYS, 2011) :
Conservation of mass equation:

$$\frac{\partial \rho}{\partial t} + \nabla.\rho\vec{v}_r = 0 \tag{5}$$

Conservation of momentum equation:

$$\frac{\partial}{\partial t}(\rho\vec{v}_r)+\nabla.(\rho\vec{v}_r.\vec{v}_r)+\rho(2\vec{\omega}\times\vec{v}_r+ \\ +\vec{\omega}\times\vec{\omega}\times\vec{r}+\vec{a}\times\vec{r}+\vec{a})=-\nabla p+\nabla\bar{\bar{\tau}}+\vec{F} \quad (6)$$

Where $\vec{a}=\frac{d\vec{\omega}}{dt}$ and $\vec{a}=\frac{d\vec{v}_t}{dt}$

The stress tensor $\bar{\bar{\tau}}$ is given by

$$\bar{\bar{\tau}}=\mu\left[\left(\nabla\vec{v}+\nabla\vec{v}^T\right)-\frac{2}{3}\nabla\vec{v}I\right] \quad (7)$$

The momentum equation incorporates four additional acceleration terms. The initial two terms represent the Coriolis acceleration ($2\vec{\omega}\times\vec{v}_r$) and the centripetal acceleration ($\vec{\omega}\times\vec{\omega}\times\vec{r}$), respectively. These terms are applicable in both steadily moving reference frames (where v_r and ω are constant) and accelerating reference frames (where v_r, and/or ω are functions of time). The third and fourth terms arise from the unsteady change in rotational speed and linear velocity, respectively. Notably, these terms become negligible in scenarios involving constant translation and/or rotational speeds.

3. Calculation models and boundary conditions

3.1 Problem geometry and computed fluid domain

The investigation in this paper focuses on a four-bladed propeller operating at an angular velocity of 200 rpm. Table 1 presents the main variables associated with the propeller, providing essential details for the research.

Table 1: Propeller detail parameters

Parameter	Value	Unit
Diameter	3.650	m
Pitch	2.459	m
Revolution	200	rpm
Pitch ratio	0.674	
Pitch ratio at 0.7	0.710	
Pitch at 0.7	2.592	m
Number of blades	4	
Expanded area	6.697	m^2
Expanded area ratio	0.640	
Blade thickness ratio	0.049	
Boss ratio	0.173	
Cross section	NACA 66, a=0.8	
Rake	10	Deg
Screw	25	Deg

For all computations, an accelerating duct featuring a NACA 4415 cross section was used. Table 2 outlines the specific parameters associated with the duct, providing comprehensive information for reference in analysis.

Table 2: Duct detail parameters

Parameter	Value	Unit
Length of duct	2.500	m
Cross section of duct	NACA 4415	
Gap between blade tip and duct	0.040	m
Angle between the cross section of duct and the propeller' axis	5	degree

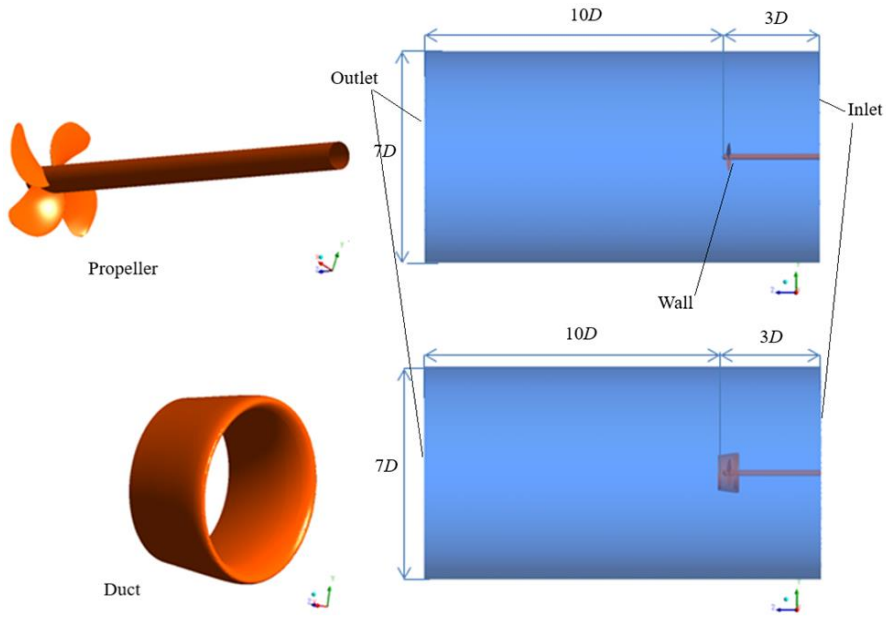

Fig. 2: The models of the propeller, duct and computed fluid domain

3.2 Computational mesh

In the exploration of the impact of the duct on hydrodynamic features of the operating propeller, the initial phase of the calculation and simulation process involves constructing the geometry model for both the free propeller and the ducted propeller system. The SolidWorks tool, renowned for its proficiency in handling complex geometries, was employed for this purpose. Subsequently, the computational domain, encapsulating both the free propeller and ducted propeller, was defined. The calculated domain takes the form of a cylinder with the length 13 times of diameter of the propeller and width 7 times the propeller's diameter. This domain is subdivided into two parts, the dynamic domain and the static domain (Baltazar and Falcao de Campos, 2009, Baltazar *et al*, 2012, Bhattacharyya *et al*, 2015, Cong *et al*, 2018, Dai *et al*, 2021, Loi *et al*, 2019, Ngo *et al*, 2015, Villa *et al*, 2020) .

The dynamic domain, representing the immediate vicinity of the propeller, is characterized by a finer mesh, while the static domain, encompassing the surrounding space, employs a coarse mesh. The meshing was executed using the ANSYS Meshing ICEM-CFD tool, employing polyhedral meshing techniques. Recognizing the pivotal role of mesh in numerical simulations, a meticulous approach was adopted to determine the optimal mesh density. Six different mesh cases were systematically evaluated, and the relationship between mesh number and the thrust coefficient of the propeller at an advance ratio J of 0.2 was analyzed. A comprehensive diagram was presented to showcase the mesh independence of simulation results. Based on this analysis, the team selected the mesh configuration from five specific cases for all subsequent calculations (Cong *et al*, 2018, Dai *et al*, 2021, Loi *et al*, 2019, Majdfar *et al*, 2017, Ngo *et al*, 2015, Villa *et al*, 2020) .

Table 3 provides detailed parameters for the chosen mesh configuration, ensuring transparency and replicability in the computational setup.

Table 3: Mesh detail parameters for free water and ducted propeller

Domain	Nodes	Elements	Polyhedral mesh
Free water propeller			
Dynamic fluid	1649594	326437	326437
Static fluid	1710639	305209	305209
All domain	3360233	631646	631646
Ducted propeller system			
Dynamic fluid	1384067	279615	279615
Static fluid	2507274	449160	449160
All domain	3976973	741617	741617

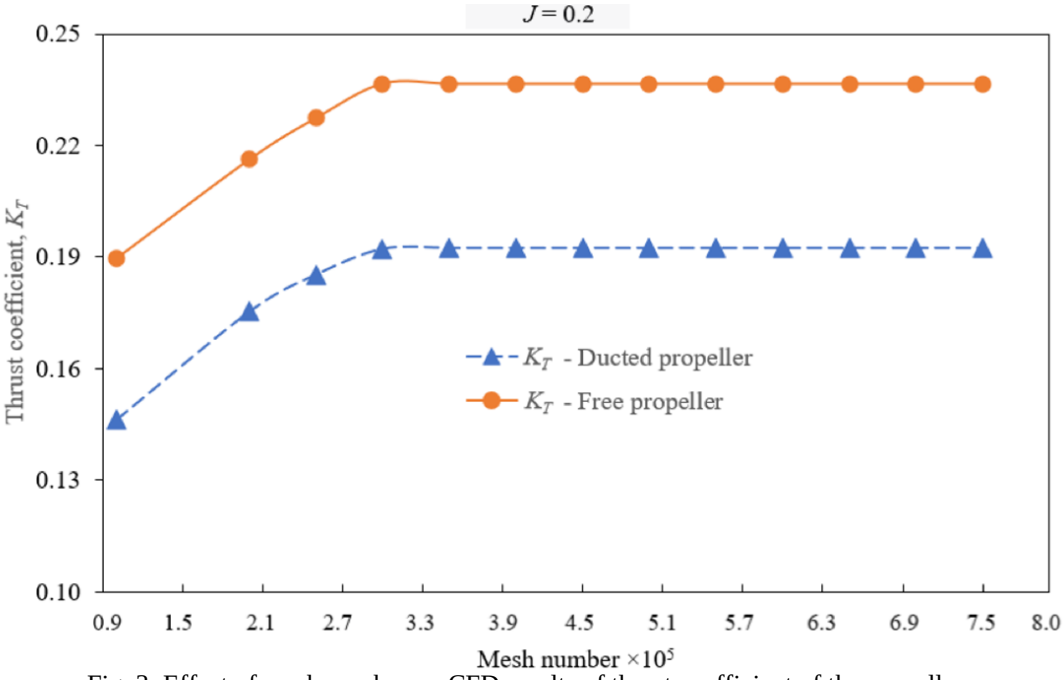

Fig. 3: Effect of mesh number on CFD results of thrust coefficient of the propeller

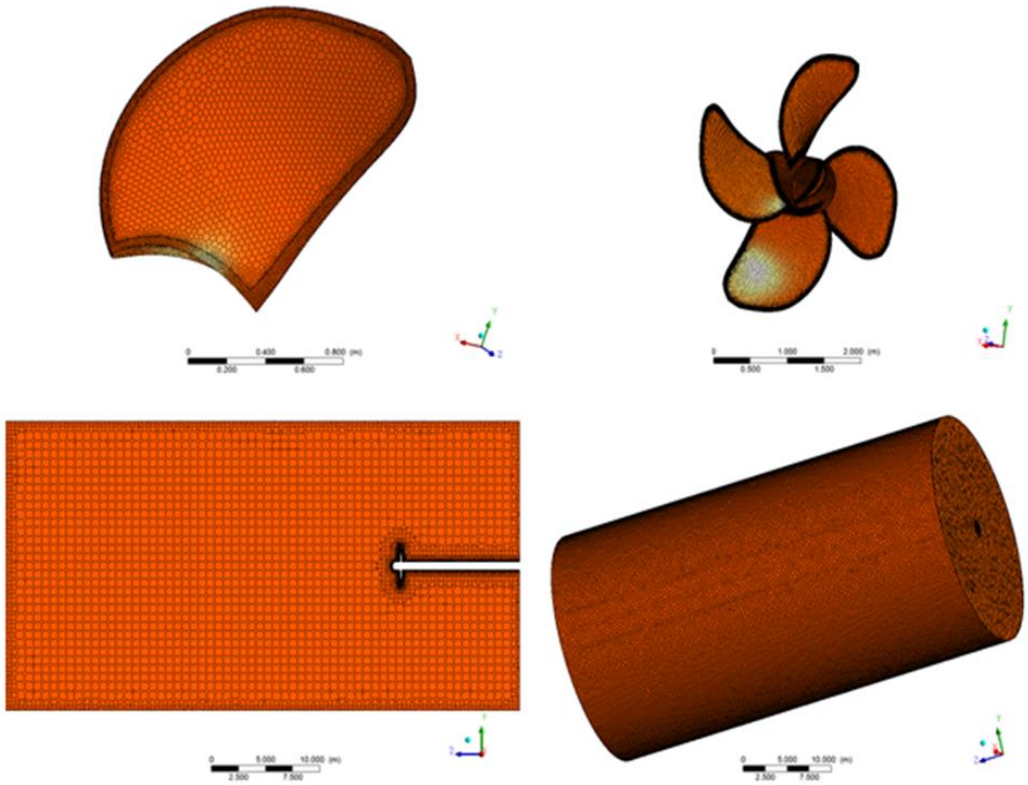

Fig. 4: Computed domain and mesh of the free propeller case

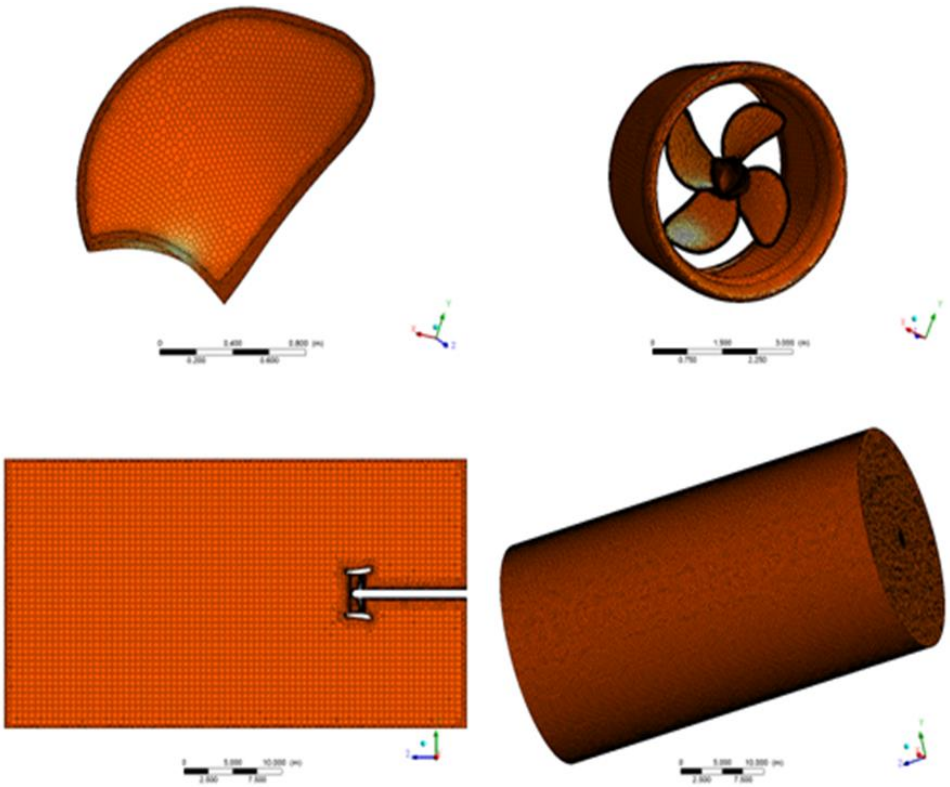

Fig. 5: Computed domain and mesh of the ducted propeller case

3.3 Calculation method and boundary condition

In this research, three turbulence models RNG k-ε, SST k- ω and the Transition SST k - ω have been strategically chosen to investigate their effects on the hydrodynamic features of the propeller. Additionally, this research focuses on assessing the influence of the duct on the propeller's hydrodynamic characteristics. The velocity inlet is selected as the boundary condition at the inlet, assuming a uniform, axial velocity equal to the ship's advance velocity. The pressure outlet condition is specified at the outlet, with the gauge pressure set to 0 *Pa*. Wall boundary conditions enforce a no-slip condition on the wall surface, complemented by the application of the standard wall function in the adjacent region of the walls (Caja *et al.* 2001, Cong *et al*, 2018, Dai *et al*, 2021, ANSYS, 2011, Loi *et al*, 2019, Majdfar *et al*, 2017, Razaghian and Ghassemi, 2016, Villa *et al*, 2020) .

To establish the moving coordinate system, a Moving Reference Frame (*MRF*) is employed and synchronized with the propeller's rotation. Two coordinate systems are utilized: one rotating with the propeller and the other fixed on the static shaft of the propeller. The discretization of the convection term utilizes the first-order upwind scheme with numerical under-relaxation, while the diffusion term employs the central difference scheme. The PISO algorithm is employed for solving the pressure velocity coupling. Convergence precision is maintained at a level below 0.0001 for all residuals. Table 4 provides a detailed overview of the boundary condition, ensuring clarity and reproducibility in the simulation setup (Caja *et al.* 2001, Cong *et al*, 2018, Dai *et al* 2021, ANSYS, 2011, Loi *et al*, 2019, Majdfar *et al*, 2017, Razaghian and Ghassemi, 2016, Villa *et al*, 2020) .

Table 4: Boundary conditions for simulation

Name	**Conditions**	**Value**	**Unit**
Inlet	Velocity inlet	1.22 - 9.15	*m/s*
Outlet	Pressure outlet	0	*pa*
Wall	Static wall	-	-
Static domain	Static fluid	-	-
Dynamic domain	Rotating	200	*rpm*

4. Results and analysis

4.1 Effects of duct on the propeller's thrust and torque

Figs. 4 and 5 depict the pressure distribution on the back and pressure faces of the studied propeller in two cases at various advance ratios. The observed pressure distribution aligns seamlessly with the principle of axial turbo machinery, wherein the pressure is higher on the back face of the propeller.

For the open-water propeller, the maximum and minimum pressure on the face of the propeller are 12000 *Pa* and -120000 *Pa*, respectively. The pressure gradually increases from the hub to the tip of the propeller blade, reaching its maximum at the blade's leading edge and the minimum at a small region near the tip. In regions where the pressure drops below the vapor pressure, cavitation may occur. On the back face, the pressure increases gradually from the blade's tip to the propeller's boss, with the maximum pressure reaching about 2.4×10^4 *Pa* at the trailing edge of the blade. The area around the blade's leading and tip experiences the minimum pressure of approximately -1.2×10^5 *Pa*, making it susceptible to cavitation. The pressure difference between the two faces generates the thrust of the propeller.

In contrast, with the ducted propeller, the pressure distribution on the blade changes rapidly. As illustrated in the Figs. 6 and 7, the pressure difference between the two faces diminishes significantly. The maximum pressure on the pressure face is around 3×10^4 *Pa*, concentrated at the blade's trailing edge, while the minimum value is about -3×10^4 *Pa*, focused on the propeller blade's leading edge and the tip. On the back face, the pressure distribution increases gradually from the tip to the boss of the propeller. The minimum pressure area on the back face is smaller than that of the open-water propeller, concentrating only on the blade's tip. The results indicate that the duct has a profound effect on the propellers' hydrodynamic characteristics, considerably reducing the pressure difference between the two faces and, consequently, lowering the propeller's thrust. However, it is noteworthy that the system's thrust, considering both the propeller and duct, is slightly smaller than the thrust of the open-water propeller, especially at small advance ratios.

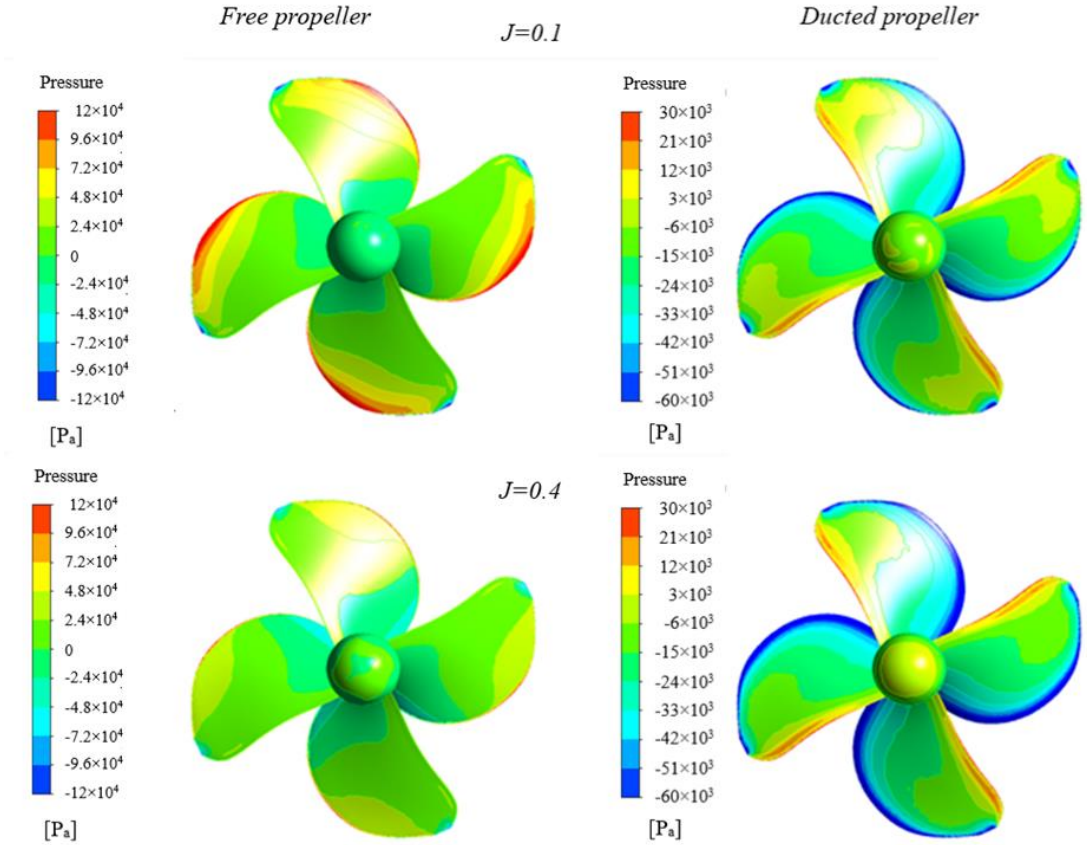

Fig. 6: Pressure distribution over surface area of the pressure faces of the open water propeller and the ducted propeller at the various advance ratios *J* of 0.1, 0.4

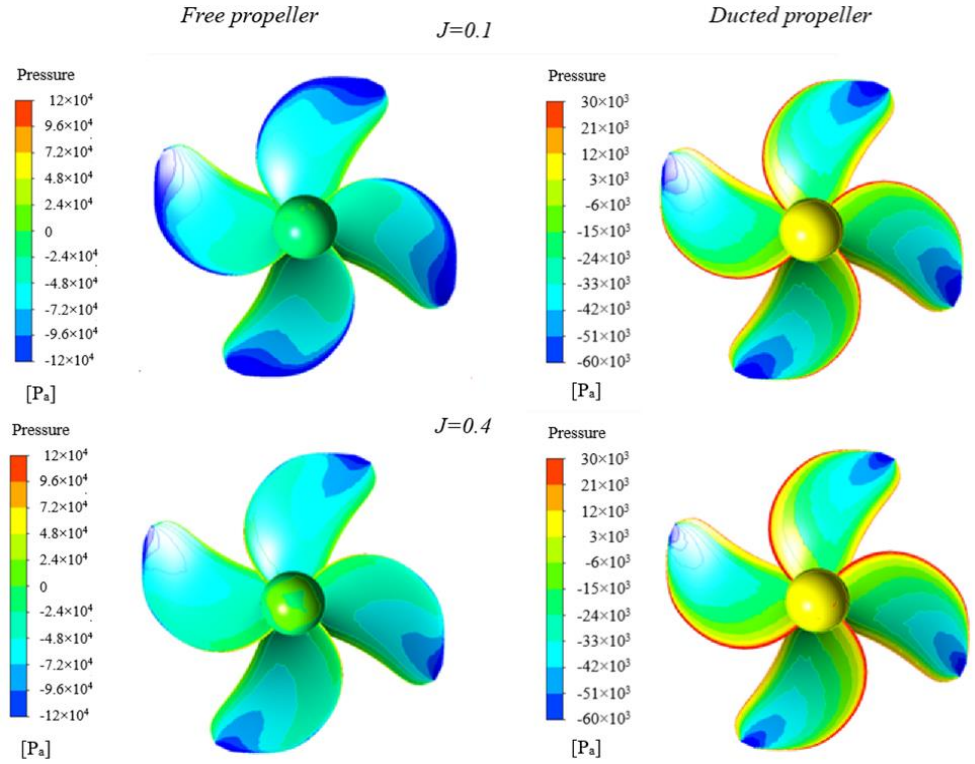

Fig. 7: Pressure distribution over surface area of the back face of the propeller at J of 0.1, 0.4

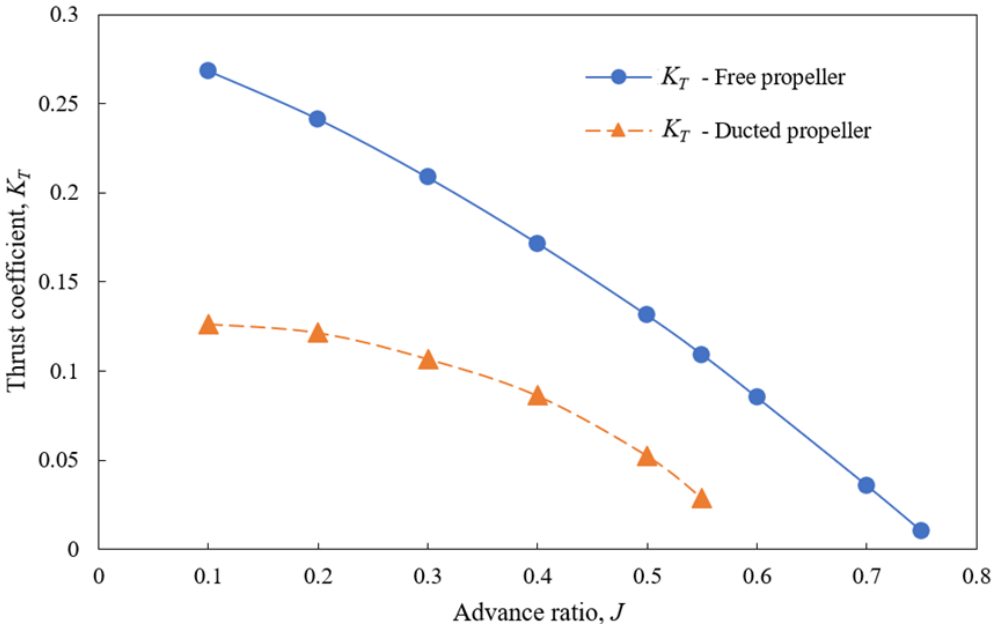

Fig. 8: Thrust coefficient of the propeller in both cases

Fig. 8 provides a comparison of the propeller's thrust coefficient at different advance ratios in two computed cases: the free propeller and the ducted propeller. Notably, the thrust coefficient of the propeller in the ducted configuration in significantly smaller than that of the free propeller, especially at lower advance ratios. At an advance ratio J of 0.1, both cases reach their maximum thrust coefficient. However, the thrust coefficient of the free propeller is approximately twice that of the ducted propeller at this specific advance ratio. This observation underscores the considerable effect of the duct on reducing the overall thrust coefficient, particularly in scenarios with lower advance ratios.

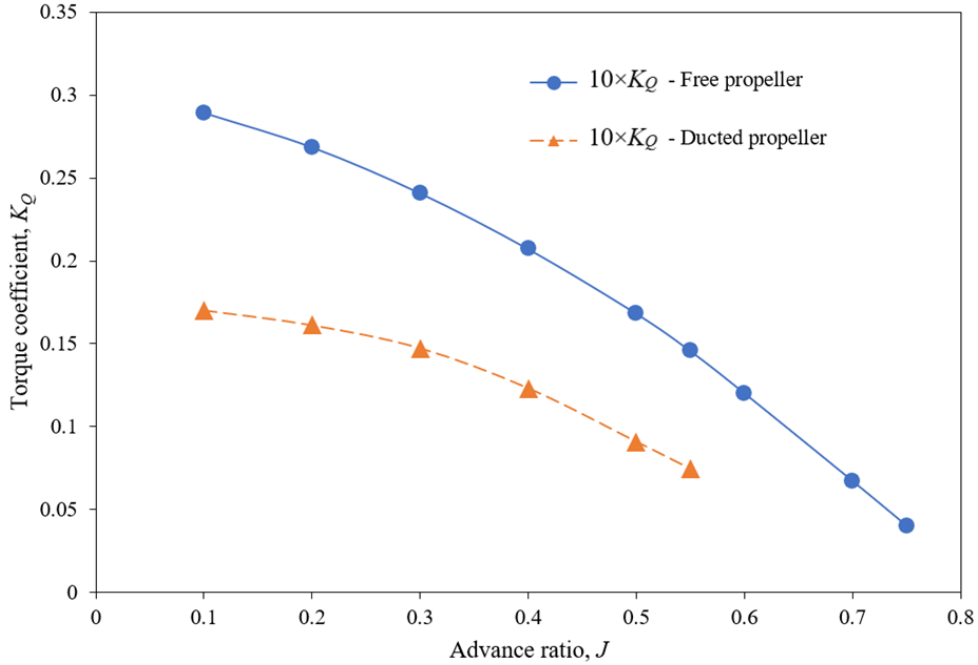

Fig. 9: Torque coefficient of the propeller in both cases

Fig. 9 illustrates the torque coefficients at different ratios in both the free propeller and ducted propeller configurations. The notable observation is that the torque coefficient of the free propeller is significantly larger than that of the ducted propeller. At their respective maximum values, the torque coefficient for the free propeller is 0.2875, while for the ducted propeller, it is 0.1665. The torque coefficients of the ducted propeller is approximately half that of the free propeller, emphasizing the substantial reduction in torque.

Interestingly, at small advance ratios J in the ducted propeller system, the reduction in torque is considerable more pronounced than that of the thrust. This results in a significant improvement in the efficiency of the ducted propeller system. The figure effectively captures the nuanced relationship between torque, advance ratio, and the effect of the duct on system efficiency.

4.2 Effects of duct on the efficiency of the propeller

Fig. 10 presents a comparative analysis of the efficiency of the studied propeller in both open-water and ducted configurations. Notably, the efficiency trends reveal interesting insights across different advance ratios.
For the open-water propeller, efficiency exhibits a gradual increase as the advance ratio escalates within the range of 0.1-0.6. The maximum efficiency for the open-water propeller is approximately 0.655, achieved at advance ratio J of 0.6.

Conversely, the ducted propeller system demonstrates a distinct efficiency profile. Its maximum efficiency is about 0.54, occurring at an advance ratio J of 0.4. Notably, at small advance ratios the efficiency of the ducted propeller is significantly higher than that of the open-water propeller. Specifically, at an advance ratio J of 0.1, 0.2 and 0.3, the efficiency of the ducted propeller is double that the open-water propeller. This suggests that the ducted propeller is particularly well-suited for application involving small velocity and heavy loads, such as tugboats and fishing trawlers. The efficiency parity at an advance ratio J of 0.4 indicates a comparable performance between the two configurations under certain operational conditions.

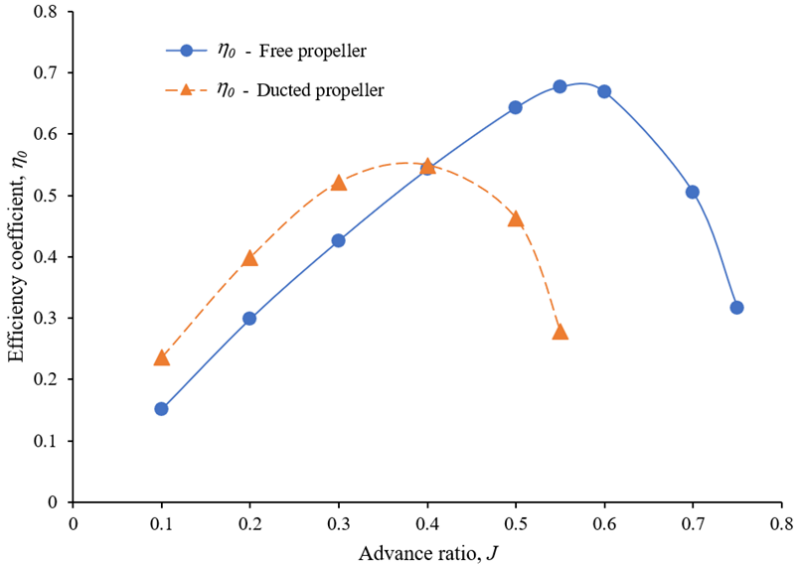

Fig. 10: Efficiency of the propeller in the two cases open-water propeller and ducted propeller

4.3 Effects of duct on the velocity field and tip vortex

Fig. 11 illustrates the velocity distribution on the axial plane and the streamline surrounding the propeller in both cases, shedding light on the distinct effects of the duct on the velocity field and tip vortex. In the case of the ducted propeller, relatively small pressure difference of the blade tip between the two faces leads to a notable reduction in backflow from the suction face to the pressure face, particularly at small advance ratios. Consequently, the tip vortex in this configuration experiences a significant decrease. This reduction in the tip vortex, especially at low advance ratios, contributes substantially to the improvement in the efficiency of the ducted propeller. The figure captures the nuanced changes in the velocity field and tip vortex dynamics, providing valuable insights into the enhanced performance of the ducted propeller in scenarios with small advance ratios.

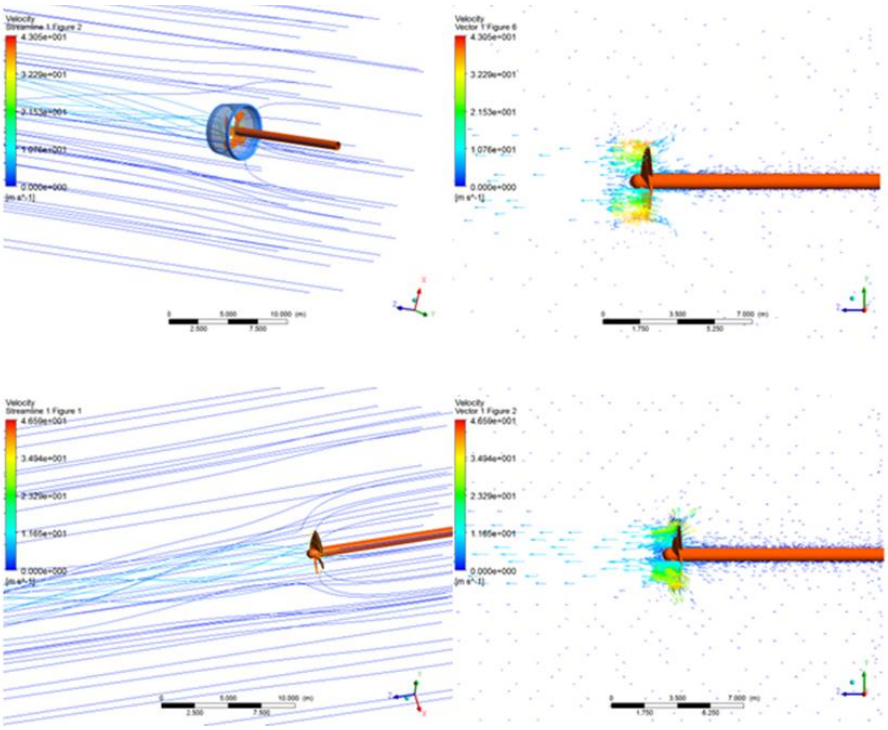

Fig. 11: Streamlines and velocity vector surrounding the propeller in both cases at J of 0.1

4.4 Force acting on the duct in operation

Fig. 12 provides insights into the pressure distribution on the duct and its thrust coefficient at various advance ratios, elucidating the forces acting on the duct during operation. The cross-sectional shape of the duct resembles that of an airfoil, inducing a pressure difference across its two faces resulting in low pressure inside the duct and high pressure outside. This pressure distribution gives rise to a hydrodynamic force on the duct, decomposed into two components: one aligning with the propeller's thrust and the other oriented along the propeller's axis. Consequently, the total thrust of the ducted propeller system comprises the thrust generated by both the duct and the propeller.

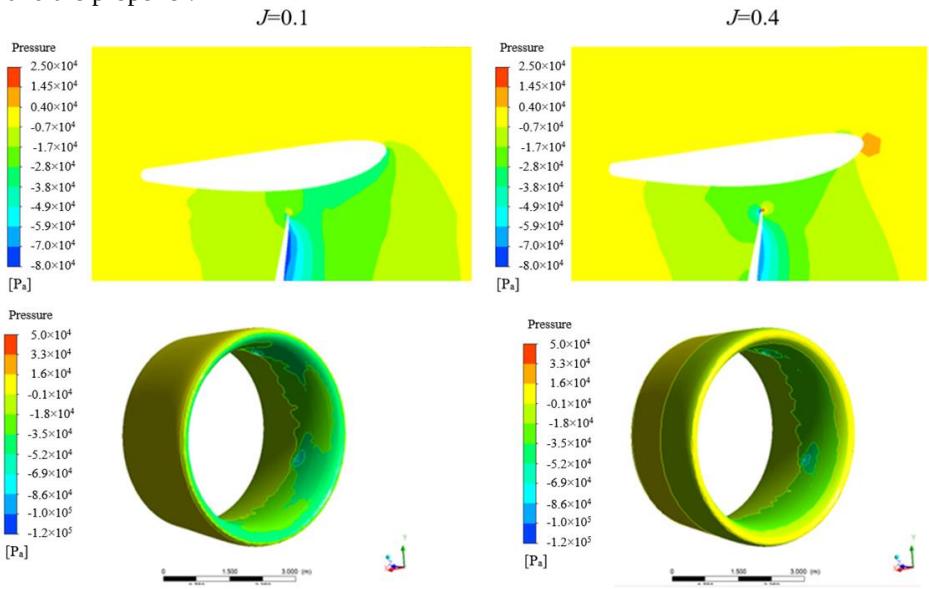

Fig. 12: Pressure distribution in computed domain and over surface area of the duct at *J* of 0.1 and 0.4

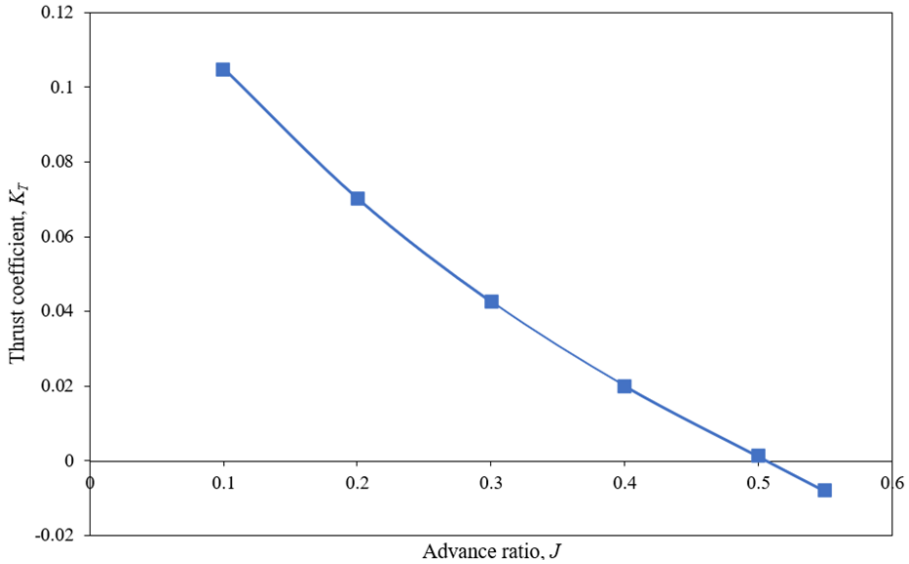

Fig. 13: The thrust coefficient of duct in the system at various advance ratios

Observing the figure, it becomes evident that as the advance ratio increases, the thrust coefficient of the duct experiences a notable decline. Its maximum value, reaching 0.13 at an advance ratio *J* of 0.1, diminishes to a minimum value of approximately -0.01 at the advanced ratio *J* of 0.55. This reduction in the duct's thrust coefficient contributes to an overall decrease in the system's thrust at higher advance ratios. In summary, the ducted propeller system proves to be particularly suitable for vessels operating at low velocities and carrying heavy loads based on the comprehensive analyses conducted.

4.5 Effects of turbulence models on CFD results

The effect of different turbulent viscous models on the CFD results is depicted in Fig. 14, revealing that the chosen turbulence viscous models shown minimal influence on the calculation results.

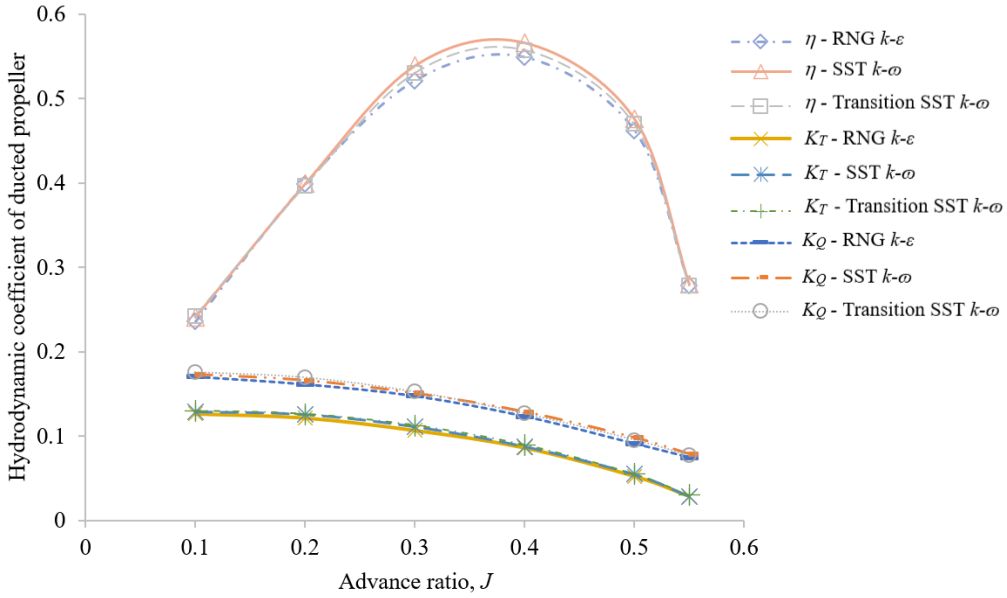

Fig. 14: Hydrodynamic characteristics at the various turbulent models

The obtained results with the k - ω SST model indicate that the propeller's efficiency peaks at approximately 0.545, while the lowest efficiency, around 0.536, is observed with the transition SST k - ω model at an advance ratio J of 0.4. Similarly, the thrust coefficient reaches its maximum value about 0.1133 with the transition SST k - ω model, and the minimum around 0.1129, is recorded using the RNG k-ε model. Regarding the propeller's torque coefficient, the highest and lowest values, approximately 0.133, 0.1317, respectively, are observed with the k - ω SST model and the transition k - ω SST model.

It is noteworthy that the error among the investigated parameters across the selected models is relatively small, approximately 1.39%. This negligible discrepancy suggests that the choice of turbulence model has minimal effects on the overall accuracy of the calculations.

5. Conclusions

This study conducts a numerical investigation and analysis of steady flows around a free-water propeller and a ducted propeller at different ratios, employing an unstructured mesh based on RANS. Several key conclusions can be drawn from this research:

- The study verifies the numerical simulation method using a four-bladed skewed propeller from the TanCang foundation ship for both open-water and ducted configurations. Numerical predictions of thrust coefficient K_T, torque coefficient K_Q, and power efficiency coefficient η at different advance ratios demonstrate a dramatic increase in propeller efficiency at small ratios, with potential improvements of up to 30 % compared to free open propeller. The numerical predictions align well with theoretical prediction, affirming the accuracy of the simulation method.
- Contour presentations of pressure distribution on the duct and blade reveal negative low pressure on the backside and high positive pressure on the face side of the blade. Lower pressure on the suction side of the duct (inside of the duct) is also observed.
- Results suggest that ships operating within a specific velocity range and under heavy load conditions, where tip vortex is significant, can benefit from equipping ducted propellers to improve efficiency.
- Three turbulence models were employed to investigate their effects on simulation results. The study concludes that the chosen turbulence models have an insignificant effect on the simulation results, allowing for their neglect in practical applications.

The study provides valuable insights into the hydrodynamic performance of propellers and ducted propellers, emphasizing efficiency improvements in specific operating conditions. The verification of numerical methods and analysis of turbulence viscous model effects contribute to a comprehensive understanding of propeller performance and aid in practical design considerations for marine applications.

Acknowledgments

The authors would like to thank the supports of the Vietnam Ministry of Education and Training under grant number B2023-BKA-13.

References

Abbott and Doenhoff, (1959): Theory of Wing Sections. Fist ed. New York, New York: Dover Publications, Inc.

Abdel-Maksoud, M., Heinke, H., (2002): Scale effects on ducted propellers, Proceedings of the 24th symposium on naval hydrodynamics, pp. 744-759.

Baltazar, J., Falcao de Campos, J., (2009): On the modelling of the flow in ducted propellers with a panel method, Proceedings of the 1st International Symposium on Marine Propulsors, pp. 1-15.

Baltazar, J., Falcão de Campos, J., Bosschers, J. (2012): Open-water thrust and torque predictions of a ducted propeller system with a panel method. International Journal of Rotating Machinery, John Wiley & Sons Ltd. https://doi.org/10.1155/2012/474785

Bhattacharyya, A., Neitzel, J.C., Steen, S., Abdel-Maksoud, M., Krasilnikov, V., (2015): Influence of flow transition on open and ducted propeller characteristics, Fourth International Symposium on Marine Propulsors, Austin, Texas, USA.

Bontempo, R., Cardone, M., Manna, M. (2016): Performance analysis of ducted marine propellers. Part I–Decelerating duct. Applied Ocean Research, 58, 322-330. https://doi.org/10.1016/j.apor.2015.10.005

Breslin, J.P., Andersen, P., 1994. Hydrodynamics of ship propellers. Cambridge university press.

Caja, A.S., Rautaheimo, P., Siikonen, T., (2001): Simulation of incompressible viscous flow around a ducted propeller using a RANS equation solver, 23rd Symposium on Naval Hydrodynamics. National Academies Press, pp. 527-539.

Cong, N.C., Loi, L.N., Van He, N. (2018): A study on effects of blade pitch on the hydrodynamic performances of a propeller by using cfd. Journal of Shipping and Ocean Engineering, 8, 36-42. https://doi.org/10.17265/2159-5879/2018.01.005

Dai, Y., Zhang, Y., Bian, J., Han, K., Zhu, X., Huang, Z., Xie, Y. (2021): CFD simulation on hydrodynamics of underwater vehicle with ducted propellers. Int. J. Simul. Model 20, 1601-1611. https://doi.org/10.2507/IJSIMM20-3-CO14

Ansys Inc. (2011): Ansys fluent theory guide, USA 15317, 724-746.

Ghassemi, H., Majdfar, S., Forouzan, H. (2016): Calculations of the hydrodynamic characteristics of a ducted propeller operating in oblique flow. Ship Science and Technology, 10 (20), 31-40. https://doi.org/10.25043/19098642.147

Kao, J.-H., Liao, Y.-F. (2022): Discussion of the fluid acceleration quality of a ducted propulsion system on the propulsive performance. CMES-Computer Modeling in Engineering & Sciences, 130 (3). https://doi.org/10.32604/cmes.2022.016212

Kerwin, J.E., Kinnas, S.A., Lee, J.-T., Shih, W.-Z. (1987): A surface panel method for the hydrodynamic analysis of ducted propellers. SNAME transactions, 95, 93-122.

Koh, K., Omar, Y., Azreen, E., Nurhaslina, K. (2015): The study of ducted propeller in propulsion performance of a Malaysia fishing boat. Journal Teknologi (Sciences & Engineering), 74 (5), 39-43. https://doi.org/10.11113/jt.v74.4639

Krasilnikov, V., Sun, J., Zhang, Z., Hong, F., (2007): Mesh generation technique for the analysis of ducted propellers using a commercial RANSE solver and its application to scale effect study, Proceedings of the 10th Numerical Towing Tank Symposium (NuTTS'07).

Lee, H., Kinnas, S., (2006): Prediction of cavitating performance of ducted propellers, Proceedings of the Sixth International Symposium on Cavitation.

Loi, L.N., Cong, N.C., Van He, N. (2019): CFD results on hydrodynamic performances of a marine propeller. Vietnam Journal of Marine Science and Technology, 19 (3), 345-447. https://doi.org/10.15625/1859-3097/19/3/13246

Majdfar, S., Ghassemi, H., Forouzan, H., Ashrafi, A. (2017): Hydrodynamic prediction of the ducted propeller by CFD solver. Journal of Marine Science and Technology, 25 (3), 3.
Majdfar, S., Ghassemi, H., Forouzan, H. (2015): Hydrodynamic Effects of the length and angle of the ducted propeller. Journal of Ocean, Mechanical and Aerospace–Science and Engineering, 25, 19-25.
Motallebi-Nejad, M., Bakhtiari, M., Ghassemi, H., Fadavie, M. (2017): Numerical analysis of ducted propeller and pumpjet propulsion system using periodic computational domain. Journal of Marine Science and Technology, 22, 559-573. https://doi.org/10.1007/s00773-017-0438-x
Ngo, V., Le, T., Le, Q., Ikeda, Y., (2015): A study on interaction effects on hydrodynamic performance of a system rudder-propeller by distant gap, Proceedings of the 12th International Marine Design Conference, Tokyo, Japan, pp. 179-193.
Razaghian, A.H., Ghassemi, H. (2016): Numerical analysis of the hydrodynamic characteristics of the accelerating and decelerating ducted propeller. Zeszyty Naukowe Akademii Morskiej w Szczecinie, 47 (119), 42-53.
Rijpkema, D., Vaz, G. (2011): Viscous flow computations on propulsors: verification, validation and scale effects. Proceedings of the Developments in Marine CFD.
Suryanarayana, C., Satyanarayana, B., Ramji, K. (2010): Performance evaluation of an underwater body and pumpjet by model testing in cavitation tunnel. International Journal of Naval Architecture and Ocean Engineering, 2 (2), 57-67. https://doi.org/10.2478/IJNAOE-2013-0020
Takinacı, A.C., Taralp, T. (2021): Prediction and simulation of broadband propeller noise. Journal of Marine Science and Technology, 21 (5), 6.
Villa, D., Gaggero, S., Tani, G., Viviani, M. (2020): Numerical and experimental comparison of ducted and non-ducted propellers. Journal of Marine Science and Engineering, 8 (4), 257. https://doi.org/10.3390/jmse8040257
Zondervan, G.-J., Hoekstra, M., Holtrop, J., (2006): Flow analysis, design and testing of ducted propellers, SNAME Propeller and Shafting Symposium. SNAME, p. D011S001R006. https://doi.org/10.5957/PSS-2006-06